Magnesium Technology 2015
Edited by: Michele V. Manuel, Alok Singh, Martyn Alderman, and Neale R. Neelameggham
TMS (The Minerals, Metals & Materials Society), 2015

Investigation of Compression Behavior of Mg-4Zn-2(Nd,Gd)-0.5Zr at 350°C by *In Situ* Synchrotron Radiation Diffraction

*R. H. Buzolin[1,2], D. Tolnai[1], C. L. Mendis[1], A. Stark[1], N. Schell[1], H. Pinto[2], K. U. Kainer[1], N. Hort[1]

[1]Institute of Materials Research, Helmholtz-Zentrum Geesthacht, Germany
Max-Planck-Strasse 1,
D 21502, Geesthacht, Germany
(*Corresponding author: ricardo.buzolin@usp.br)

[2]Department of Material Engineering, University of Sao Paulo, Brazil
Av. Joao Dagnone, 1100 Jd. Sta Angelina,
13563-120, Sao Carlos, Brazil

Keywords: ZK40, RE additions, deformation behaviour, *in situ*, synchrotron radiation

Abstract

As-cast Mg-4Zn-0.5Zr, Mg-4Zn-2Gd-0.5Zr and Mg-4Zn-2Nd-0.5Zr alloys were investigated by *in situ* synchrotron radiation diffraction during hot compression at 350 °C using the facilities of P07 beamline of Petra III at Deutsches Elektronen Synchrotron (DESY), Hamburg, Germany. The specimens were heated at a rate of 100 K/min and compressed with an initial strain rate of 1.1 x 10^{-3} s^{-1} up to 30 % strain. The addition of rare earth elements improved the yield strength from 23 MPa in the Mg-4Zn-0.5Zr alloy up to 40 MPa in the alloy with Nd and Gd. Continuous dynamic recrystallization played an important role in the Mg-4Zn-0.5Zr alloy during deformation and twinning was not dominant. Discontinuous dynamic recrystallization was observed in the in the Mg-4Zn-2Gd-0.5Zr along the grain boundary regions while the grains remained largely without any recrystallization. In the Mg-4Zn-2Gd-0.5Zr and Mg-4Zn-2Nd-0.5Zr alloys the contribution of twinning to deformation was observed at 350 °C. Reasons for these differences will be discussed with respect to microstructures of the alloys.

Introduction

The increased demand from the automotive industry for weight reduction and more environmentally-friendly materials, with a view to reduce exhaust gases, has initiated research in the field of lightweight materials, especially in Mg alloys [1]. Significant research is still needed on processing, alloy development, joining, surface treatment, corrosion resistance and mechanical properties improvement of Mg alloys.

Conventional magnesium alloys exhibit poor formability at ambient temperatures [2], due limited number of independent active slip systems available at room temperatures to allow an arbitrary shape change. Even though Mg alloys display some plasticity at room temperature, especially with a finer grain size and through solute additions, [2], wrought processing, such as extrusion, rolling or forming are problematic at room temperatures. Therefore, higher temperatures (>225 °C) have been used to deform Mg alloys, at which non-basal slip and deformation twinning can be activated [3].

Wu et al. [4] investigated the compression behaviour of ZK60 Mg alloy at different temperatures and found out that 250-350 °C was the most suitable range of temperature for the ZK60 alloy. The microstructure was more homogeneous at this range of temperature and exhibited almost no twins with hot compression temperature greater than 350 °C. 350 °C is a typical extrusion temperature for ZK alloys [2], thus understanding the deformation behavior of the ZK based alloys at 350°C is of importance for future alloy development.

ZK alloys are one of the high strength wrought magnesium alloys that are commercially available and are also used in the cast form. The addition of Rare Earth (RE) elements to these alloys [5] results in improved castability and elevated temperature strength [6]. RE additions refine grain size mainly due to constitutional supercooling [7]. Furthermore they weaken the anisotropy thus improve the ductility of Mg alloys [8]. Therefore, Mg-Zn-RE-Zr system is of great interest for research.

In situ high energy X-ray diffraction (HEXRD) is a unique method to investigate the dynamic microstructural processes during mechanical loading in the bulk of the materials [9]. Azimuthal-angle vs. Time plots (AT-plots) hold information about grain size evolution, grain imperfection, grain rotation, and grain orientation relationships, texture evolution. These can be correlated with crystallographic slip due to dislocation motion, sub-grain formation, twinning, recrystallization, recovery and grain growth; which are the responsible physical processes for the microstructural changes associated with deformation [9].

The present work investigates the influence of Gd and Nd addition on the compression behaviour of the ZK40 alloy combining *in-situ* radiation synchrotron study, which provides new insights into the real-time evolution of the microstructure, and electron backscattered diffraction (EBSD) in order to study the deformed structure.

Experimental Procedures

The alloys were prepared by permanent mould indirect chill casting [10] with nominal compositions Mg4Zn-0.5Zr (Mg2.2Zn-0.14Zr) Mg-4Zn-0.5Zr-2Gd (Mg2.2Zn-0.14Zr-.65Gd) and Mg-4Zn-0.5Zr-2Nd (Mg2.2Zn-0.14Zr-0.70Nd) in wt.% (at.% compositions are shown in brackets). The actual chemical compositions in wt.% are listed in Table 1. The Gd was added as an Mg-4 wt.%Gd alloy. The Nd was added as pure element. The melt was held at 750 °C for 10 min and then poured into a mould preheated to 660 °C and held for another 15 min in another furnace at 660 °C for final cooling with water. The permanent mould direct chill casting procedure was used for a homogeneous

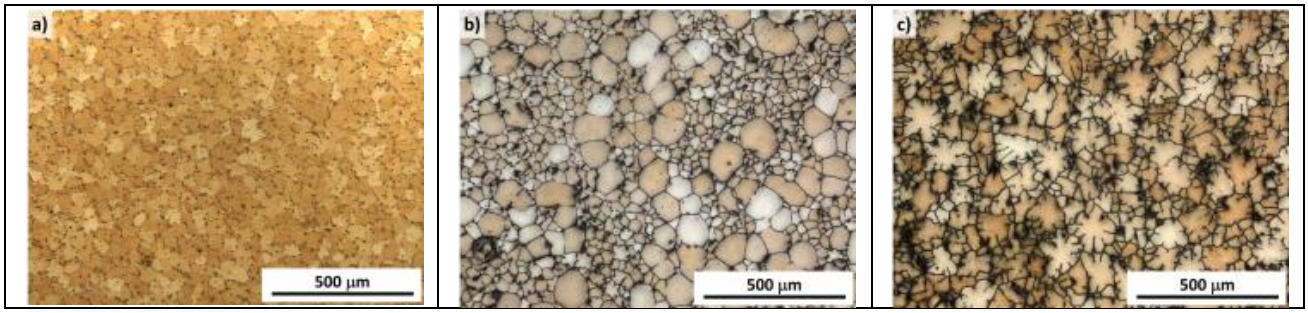

Figure 1: Optical micrographs typical of as-cast (a) ZK40; (b) ZK40-2Gd; (c) ZK40-2Nd.

distribution of alloying additions. The specimens for the *in situ* compression were machined with 5 mm diameter and 10 mm length.

For metallographic characterization of the as-cast and the deformed samples, they were mounted in epoxy and ground using SiC paper down to 2500 grit and then polished using 3 μm diamond solution. OPS solution with 1 μm diamond suspension was used as the last step of polishing. The specimens for optical microscopy (OM) were etched with acetic-picral solution and the specimens for EBSD were washed with 0.5 vol% nitric acid in ethanol solution for 5 seconds.

The optical analyses were performed using the light optical microscopy Leica DMI 5000. The SEM used was a Zeiss FEG-SEM Ultra 55 attached with a Hikari detector and a TSL-OIM software package for EBSD analysis. The measurements were performed at a voltage of 15 kV using a working distance of 13 mm and an area of 80 μm x 80 μm using a step size of 0.1μm.. The maps were measured in the centre of the deformed specimen to ensure a similar area to that measured during diffraction analysis

In-situ synchrotron high energy X-ray diffraction has been performed using the facilities of DESY (Deutsches Elektronen-Synchrotron) at P07 – Petra III with a beam having an energy of 100 keV (λ=0.124 nm) and a cross section of 1.0 mm x 1.0 mm. Diffraction patterns were recorded at a frame rate of 1/s by a PerkinElmer 1621 flat panel detector (200 μm x 200 μm) which was placed at a distance of 1535 mm from the specimen position. The acquisition time was 1.0 s. the detector to sample distance was calibrated with a LaB_6 standard powder sample and the software Fit2D® was used for evaluating the data.

The compression specimens were mounted into a chamber of a dilatometer DIL 805A/D (TA Instruments, Hüllhorst, Germany), combined with an induction coil modified so the beam can pass through the sample [11]. The specimens were heated to the intended temperature (350 °C) at a rate of 30 $°Cs^{-1}$ and held at this temperature for 3 min before the compression started. The specimens were compressed with a constant deformation speed of 0.01 mms^{-1} and the tests were carried out up to 0.3 of strain. The Debye-Scherrer rings were then analysed using Fit2D software. Selected reflections throughout the whole experiment were converted to azimuthal angle – time (A-t) plots whereas the grey scale represents the intensity from white (0) to black (high intensity).

Results

The optical micrographs of the as-cast ZK40, ZK40-2Gd and ZK40-2Nd alloys are presented in Figure 1. The ZK40 and the ZK40-2Gd alloys exhibited cellular structures whereas the ZK40-2Nd showed a more pronounced dendritic structure. The ZK40-2Gd alloy exhibited a heterogeneous microstructure with coarse grains surrounded by fine grains. For the ZK40-2Gd and ZK40-2Nd alloys the intermetallic phases were semi-continuously distributed along the grain boundaries, whereas the ZK40 had small eutectic compounds along the grain boundaries.

Table 1: The chemical compositions of the alloys investigated.

Chemical Composition				
Alloys	Gd %wt	Nd %wt	Zn %wt	Zr %wt
ZK40	-	-	5.00	0.53
ZK40-2Gd	1.70	-	4.50	0.55
ZK40-2Nd	-	2.35	4.60	0.50

The true stress-strain curves for the *in situ* compression tests are shown in Figure 2. ZK40 exhibited a 0.2% proof stress of 23 MPa and a maximum stress of 28 MPa. For the ZK40-2Gd alloy and ZK40-2Nd alloy, an increase in both the 0.2% proof stress and the maximum stress was observed. For the ZK40-2Gd alloy maximum stress and 0.2% proof stress were 56 and 40 MPa respectively and for ZK40-2Nd alloy they were 47 MPa and 39 MPa, respectively. In addition, the alloys modified with Gd or Nd show reduction in applied stress after reaching the maximum stress which was not evidenced in the ZK40 alloy.

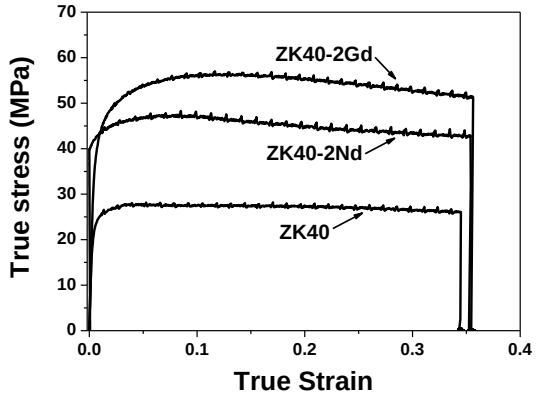

Figure 2: Compressive true stress strain curves alloys investigated at 350 ^oC

The Debye-Scherrer rings recorded during the *in situ* synchrotron radiation compression tests were converted into azimuthal-time plots to investigate the phenomena that are ongoing during the deformation and are shown in Figure 3. The planes of interest were the $\{11\bar{2}0\}$ and the $\{10\bar{1}3\}$ as twinning can be observed comparing the timelines evolution for these planes. Figures 3 (a), 3 (b) and 3 (c) display the AT-plots for the ZK40, ZK40-2Gd and ZK40-2Nd, respectively. Blurring of the timelines after the initial stages of compression is observed for the ZK40 alloy. The ZK40-2Nd alloy differs at the initial stages, where thicker timelines can be observed and the blurring of the timelines occurred at a higher strain than for the ZK40. The ZK40-2Gd does not show pronounced blurring of the timelines. The appearance of new timelines and dots in the AT-plots and the thickening of these spots after the initial stages can be observed for the ZK40-2Gd. The change in the intensity of the coupled pairs of diffraction lines $\{11\bar{2}0\}$-$\{10\bar{1}3\}$ indicate tensile twinning in Mg. The maximum normalised values of these peaks are plotted against the deformation in Figure 4. It is noted that all alloys show increase in intensity of one reflection with a corresponding decrease in the other, which is representative of tensile twinning.

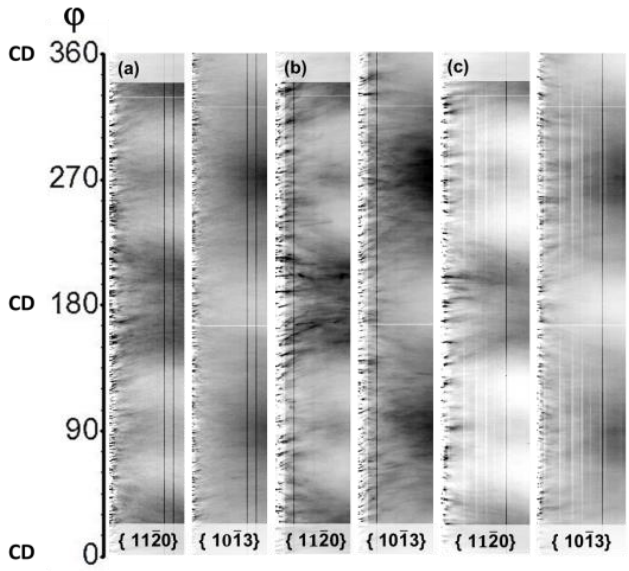

Figure 3: AT-plots derived from the *in situ* synchrotron radiation diffraction during compressive deformation of (a) ZK40, (b) ZK40-2Gd and (c) ZK40-2Nd alloys. CD represents the compression direction.

The SEM micrographs of the deformed microstructures are shown in Figure 5. The red circles highlight the areas where the fracture of the intermetallic particles was observed for the ZK40-2Gd alloy (Figure 5 (b)) and ZK40-2Nd alloy (Figure 5 (c)). This was not observed for the ZK40 alloy (Figure 5 (a)).

EBSD inverse pole figure maps are shown in Figure 6. The ZK40 contain recrystallized grains along the grain boundaries, region A in Figure 6 (a). Sub-grain formation is observed in region B while no tensile twins were observed. The ZK40-2Gd contains a significant number of recrystallized grains at the grain boundary as indicated by C, Figure 6 (b). In addition, tensile twins are observed in the final microstructure, region D. Tensile twins were also observed in the ZK40-Nd, Figure 6 (c). However, almost no recrystallized grains at the grain boundaries were observed for ZK40-Nd. In order to investigate in more details the sub-grain formation, grain reorientation average deviation (GROD) maps was used to study the effect of recrystallization on the microstructure of the alloys and are shown in Figure 6 (d-f). GROD maps show the deviation in orientation of a measurement point from the average orientation of the grain to which the point belongs [12]. The highest misorientation values were observed for the ZK40-2Gd alloy, whereas the lowest was for the ZK40 alloy. The highest values are at the grain boundary and the large misorientation is observed for the alloys modified with Gd or Nd addition.

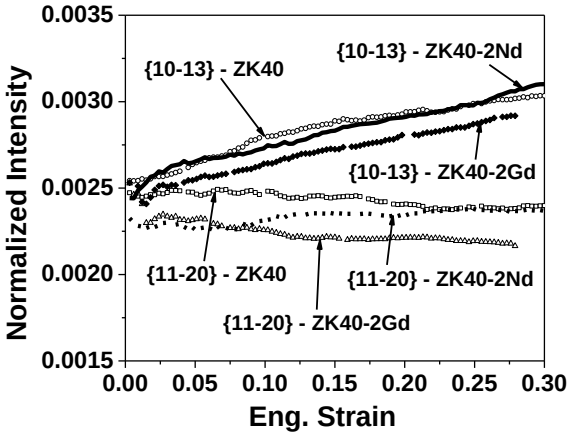

Figure 4: Change in the intensity for the $\{11\bar{2}0\}$ and $\{10\bar{1}3\}$ reflections during compressive deformation.

Discussion

In an *in situ* experiment it is possible to investigate the evolution of various deformation, recovery and recrystallization mechanisms and the manner they act during compression. There are essentially four phenomena that are observed on the AT-plots: recrystallization; recovery, which was not clearly observed for the alloys in study; grain rotation, which is shown by the bending of the timelines, and grain growth, which is very unlikely to happen during deformation. In addition, the discrete timelines correspond to individual grains. Investigating the AT-plots (Figure 3) an intensive recrystallization is noticeable at the initial stages, which is showed by the appearance of new timelines. Subsequently, the timelines bend due to the rotation of the grains by the reason of the plastic deformation process. Afterwards, these timelines blur as a result of the great amount of sub-grain formation. Eventually, the reflections broaden, merging into the final texture of the material. Such sequence is common for the three alloys investigated.

The impact on the mechanical behaviour during compression at 350 ^{o}C of the addition of Gd or Nd was significant as indicated by the increase in the 0.2% proof stress and maximum stress measured for ZK40-2Gd ZK40-2Nd alloys, Figure 2. The intermetallic particles were partially broken by cleavage for the ZK40-2Gd and ZK40-2Nd during compression, indicating that and these particles hinder the stress transfer between grains at the grain boundaries.

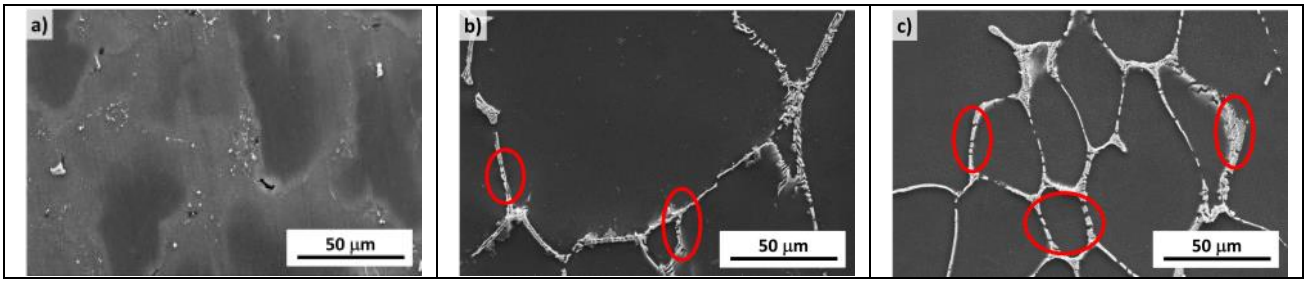

Figure 5: SEM micrographs of the deformed microstructures showing cracks in intermetallic particles (a) ZK40, (b) ZK40-2Gd and (c) ZK40-2Nd.

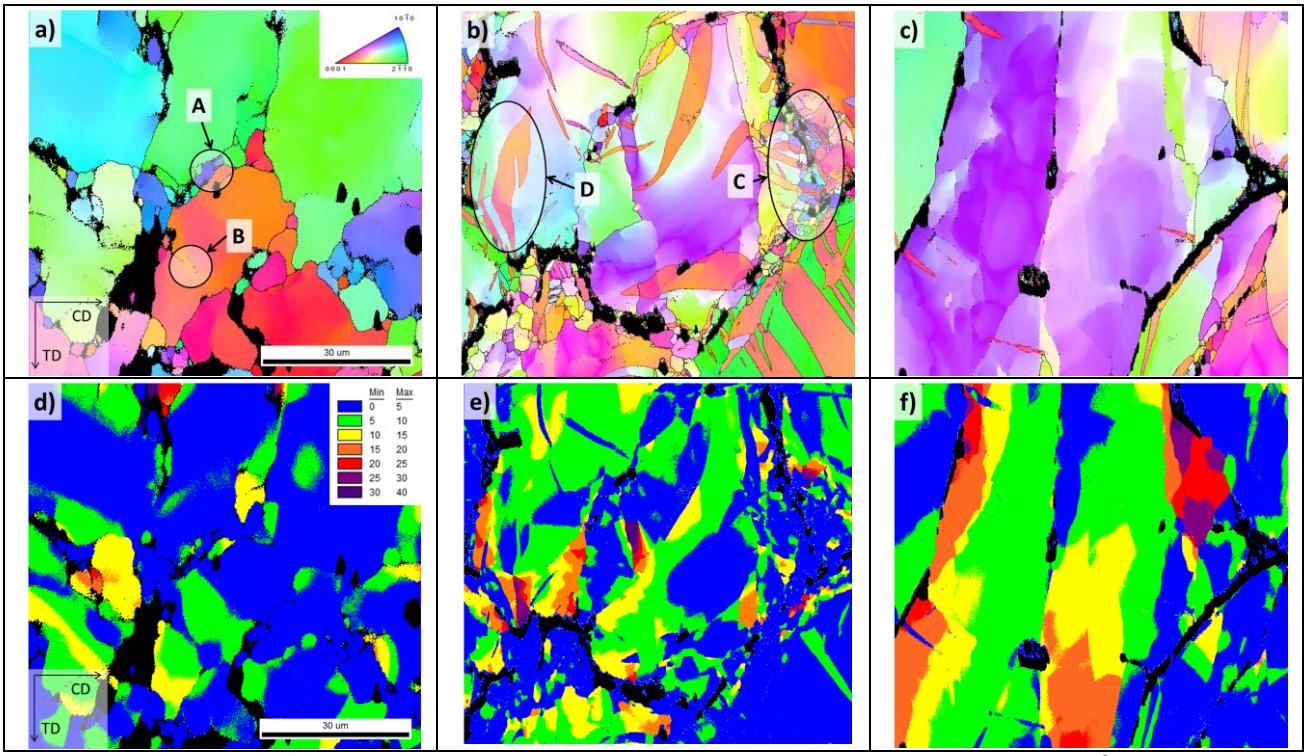

Figure 6: (a-c) EBSD inverse pole figure maps of samples after a total compressive strain of 30% at 350 ^{o}C and (d-f) Grain reorientation deviation maps for the same areas as in (a-c) (a, d) ZK40, (b, e) ZK40-2Gd and (c, f) ZK40-2Nd.

In the ZK40 alloy recrystallization is more pronounced from the early stages of deformation. It is possible that some grains had twinned because theirs orientation was energetically favourable. However, such event was not pronounced for this alloy and residual twins were not observed in the inverse pole figure map, Figure 6 (a). The highly deformed and elongated grains of the ZK40 alloy, Figure 6 (a), exhibited a large fraction of sub-grains highlighted in region B.

In the case of the ZK40 alloy no intermetallic phases hinder the grain boundary which allows grain sliding, thus lowering the energy stored at the grain boundary during deformation, which was not favourable for twinning. However, the changes of the maximum value of selected diffraction lines of the integrated line profiles during deformation show presence of some twinning. The decrease of the intensity of the $\{11\bar{2}0\}$ and increase of the intensity $\{10\bar{1}3\}$ indicates increase in the twin volume fraction. It is noted in Figure 6 (d) that the smallest GROD values was found for the ZK40, highlighting the impact of the particle pinning the grain boundary of ZK40-2Gd and ZK40-2Nd alloys. This is likely to be one of the reasons, twinning was more favourable for alloys with GD and Nd; and responsible for the higher strength observed.

AT plots of ZK40-2Gd alloy, Figure 3 (b), shows that the timelines are thicker which suggest that the CDRX was not so pronounced for this alloy. In addition, the number of new timelines that appear during the intermediate stages of deformation is much higher than for the other alloys, which explain the higher volume of recrystallized grains found along the grain boundaries. On the other hand, the ZK40-2Nd alloy shows AT plot similar to that of ZK40, Figure 3. For the ZK40-2Gd alloy the less pronounced activity of the CDRX caused a higher strength compared with the ZK40-2Nd, which exhibit a higher activity as observed in Figure 3 (b).

Conclusion

In situ synchrotron radiation diffraction was performed for as-cast specimens of ZK40, ZK40-2Gd and ZK40-2Nd at 350°C and results reveal that the deformation mechanisms differ between the ZK40 and the alloys modified with Nd or Gd addition. CDRX is observed for all alloys to some extent, evidenced by the sub-grain formation and the blurring of the timelines in the AT-plots. CDRX was more pronounced for the ZK40 alloy compared with the other alloys. The broadening of the reflections for the ZK40 alloy suggests the grains had more freedom to slide than for the modified alloys. The intermetallic phases of the modified alloys and the presence of twinning and lack of recrystallization and recovery observed in ZK40-2Nd and ZK40-2Gd alloys are responsible for the enhanced maximum strength.

Acknowledgements

The authors acknowledge the Deutsches Elektronen-Synchrotron (DESY) for the provision of facilities within the framework of proposal I20130434. RB acknowledges University of Sao Paulo for granting the fellowship *´Bolsa Empreendedorismo´* and Helmholtz-Zentrum Geesthacht (HZG) for financial support during his stay in Germany.

References

1 M. O. Pekguleryuz, K. U. Kainer, A. A. Kaya, eds. *Fundamentals of magnesium alloy metallurgy* (
Philadelphia, PA, USA: Woodhead Publishing, 2013).

2 M. M. Avedesian, H. Baker, *Magnesium and magnesium alloys* Metal Park, OH, USA: *ASM Speciality Handbook*, (ASM International, 1999).

3 M. H. Yoo, *et al.*, *´´Non basal deformation modes of HCP metals and alloys: Role of dislocation source and mobility,´´ Metall. Mater. Trans A*, 33 (2002), 813-822.

4 Y. Wu, *et al.*, *´´Flow Behavior and microstructure of ZK60 magnesium alloy compressed at high strain rate´´. Trans. Nonferrous Metals Soc China*, 24 (2014), 930-939.

5 T. E. Leontis, *"Magnesium and Magnesium Alloys - The Room and Elevated Temperature Properties of Some Sand Cast Magnesium-base Alloys Containing Zinc," Transactions of the Metallurgical Society of AIME*, 185 (1949), 327.

6 Q. Li, Q. Wang, Y. Wang, X. Zeng, W. Ding, *"Effect of Nd and Y addition on microstructure and mechanical properties of as-cast Mg–Zn–Zr alloy," J Alloys and Compd*, 427.1 (2007), 115-123.

7 M. B. Yang, *et al.*, "*Microstructure, tensile and creep properties of as-cast Mg-3.8Zn-2.2Ca-xCe (x=0, 0.5, 1 and 2 wt.%) magnesium alloys*," *J Rare Earths*, 30 (2012), 181-188.

8 N. Stanford *et al.*, *"Effect of microalloying with rare-earth elements on the texture of extruded magnesium-based alloys," Scripta Mater.*, 59.7 (2008), 772-775.

9 K.-D. Liss, and K. Yan., *"Thermo-mechanical processing in a synchrotron beam," Mater. Sci. Eng.: A*, 528.1 (2010), 11-27.

10 F. R. Elsayed, *et al., "Magnesium Permanent Mold Castings Optimization"* Mater. Sci. Forum 690 (2011), 65-68.

11 D. Tolnai, *et al. "Study of the solidification of AS alloys combining in situ synchrotron diffraction and differential scanning calorimetry" Mater. Sci. Forum*, 765 (2013), 286-290.

12 S .I. Wright, M. M. Nowell, and D. P. Field, "*A Review of Strain Analysis Using Electron Bakcscatter Diffrection," Microscopy and Microanalysis*, 17 (2011), 316-329.